

# Endoscopic photoconversion reveals unexpectedly broad leukocyte trafficking to and from the gut

Angela M. Morton<sup>a</sup>, Esen Sefik<sup>a</sup>, Rabi Upadhyay<sup>b</sup>, Ralph Weissleder<sup>b</sup>, Christophe Benoist<sup>a,1</sup>, and Diane Mathis<sup>a,1</sup>

<sup>a</sup>Division of Immunology, Department of Microbiology and Immunobiology, Harvard Medical School, Boston, MA 02115; and <sup>b</sup>Center for Systems Biology, Massachusetts General Hospital, Boston, MA 02114

Contributed by Diane Mathis, March 26, 2014 (sent for review March 17, 2014)

**Given mounting evidence of the importance of gut-microbiota/immune-cell interactions in immune homeostasis and responsiveness, surprisingly little is known about leukocyte movements to, and especially from, the gut. We address this topic in a minimally perturbant manner using Kaede transgenic mice, which universally express a photoconvertible fluorescent reporter. Transcutaneous exposure of the cervical lymph nodes to violet light permitted punctual tagging of immune cells specifically therein, and subsequent monitoring of their immigration to the intestine; endoscopic flashing of the descending colon allowed specific labeling of intestinal leukocytes and tracking of their emigration. Our data reveal an unexpectedly broad movement of leukocyte subsets to and from the gut at steady state, encompassing all lymphoid and myeloid populations examined. Nonetheless, different subsets showed different trafficking proclivities (e.g., regulatory T cells were more restrained than conventional T cells in their exodus from the cervical lymph nodes). The novel endoscopic approach enabled us to evidence gut-derived Th17 cells in the spleens of K/BxN mice at the onset of their genetically determined arthritis, thereby furnishing a critical mechanistic link between the intestinal microbiota, namely segmented filamentous bacteria, and an extraintestinal autoinflammatory disease.**

mucosal immunology | cell migration | autoimmunity | imaging

Interactions between the gastrointestinal microbiota and the immune system, particularly their impact on the initiation and progression of autoimmune and inflammatory diseases, are garnering much attention of late (1). Aberrant accumulation of leukocytes in the intestine is a cardinal feature of inflammatory bowel disease, a build-up that reflects, at least in part, an influx of immune cells (2). In addition, gut-microbiota/leukocyte cross-talk influences systemic immune responses, in particular extraintestinal autoimmune diseases. For example, it has been reported that one bacterial species, segmented filamentous bacteria, can protect female nonobese diabetic (NOD) mice from development of autoimmune diabetes (3) yet drive inflammatory arthritis in the K/BxN mouse model (4).

The intestinal tract is a site of frequent antigenic challenge, whether dietary or microbial, and therefore needs to be continuously replenished with circulating cells to optimize immune responses to would-be pathogens. Indeed, a few recent studies have demonstrated that blood-circulating Ly6C<sup>hi</sup> monocytes continually enter the healthy colon and subsequently differentiate in situ into tissue macrophage or dendritic cell populations (5–7). T cells are “imprinted” for gut homing primarily in the mesenteric lymph nodes (MLNs), entering the intestine via recirculation from the blood, which is facilitated by mucosal addressin cell-adhesion molecule-1 and C-C motif chemokine ligand 25 (8).

Concerning the other direction, exit from the gut, much less is known, although it is widely considered that there is little movement of leukocytes beyond the MLNs. It was recently shown that, at steady state, the intestinal microbiota controls transport of both pathogenic and commensal bacterial antigens from the gut lumen to the MLNs, which relies on ferrying by

mononuclear phagocytes (9). More generally, most investigators adhere to the concept that both cells and antigens drain from the gut directly into the MLNs. Many years ago, however, dye-tracking experiments established that the gastrointestinal tract is serviced by a series of LNs—at least five discrete entities—and specific regions of the gut are drained by particular nodes (10, interpreted as per ref. 11).

Given ample indications of a role for leukocyte migration in enteric diseases, surprisingly little is known about gut-associated immune-cell trafficking. Additionally, the interpretation of much of the existing data has been complicated by the systems used: notably, transfer models. To our knowledge, no one has yet reported specific, in vivo labeling of physiological frequencies of gut-resident leukocytes and subsequent monitoring of their migratory capabilities. Here, we report optimization of a means to follow immune-cell migration to and from the gut in a minimally perturbant manner. Upon exposure to violet light, the photoconvertible fluorescent protein, Kaede, irreversibly changes in color from green to red, so that cells are punctually tagged at the site of photoconversion. A line of mice expressing Kaede in all cell-types was engineered, and has already been used to monitor immune-cell migration from the lymphoid organs or the skin (12–15). Some of the advantages of this system are that it permits precise delineation of the origin of migratory populations, is amenable to the study of cell efflux as well as influx, allows simultaneous analysis of a multitude of migratory cell subsets as they traffic to numerous locations, and is very sensitive.

Using the standard Kaede transgenic (tg) mouse system, as well as a novel endoscopic adaptation of it, we have performed a series of experiments tracking movement of leukocytes to and from the intestine. The following major questions were addressed:

## Significance

**Gut-microbiota/immune-cell interactions play important roles in immune system homeostasis and responsiveness, but surprisingly little is known about the movement of immune cells into and, particularly, out of the gut. We used a minimally invasive system to monitor immigration of diverse innate and adaptive immune-cell types to the intestine from a distant lymph node, and a novel endoscopic adaptation of the system to follow their emigration from the distal colon to nearby and distal lymphoid organs. We uncovered an unexpectedly broad movement of leukocytes to and from the gut at steady state, as well as subset-specific migration proclivities. Moreover, we evidenced a critical cellular link between an intestinal microbe, segmented filamentous bacteria, and an extraintestinal autoinflammatory disease, the K/BxN model of arthritis.**

Author contributions: A.M.M., R.W., C.B., and D.M. designed research; A.M.M., E.S., and R.U. performed research; A.M.M. and R.U. contributed new reagents/analytic tools; A.M.M., C.B., and D.M. analyzed data; and A.M.M., R.W., and D.M. wrote the paper.

The authors declare no conflict of interest.

<sup>1</sup>To whom correspondence may be addressed. E-mail: cbdm@hms.harvard.edu or dm@hms.harvard.edu.

This article contains supporting information online at [www.pnas.org/lookup/suppl/doi:10.1073/pnas.1405634111/-DCSupplemental](http://www.pnas.org/lookup/suppl/doi:10.1073/pnas.1405634111/-DCSupplemental).

To what extent do immune cells circulate into and out of the gut under physiological conditions? Do migration patterns vary between different immune-cell lineages or lymphoid-cell functional subsets? Is it possible to visualize the arrival of colon-derived immune cells at a pathogenetically important site in a gut-distal autoimmune disease?

## Results

**Establishment of Minimally Perturbant Methodology to Monitor Leukocyte Trafficking to and from the Gut.** The Kaede tg mouse line provides the possibility of noninvasively tracking immune-cell trafficking over a timescale of 1 to 3 wk (12). As anticipated, given that expression of the Kaede reporter is driven by  $\beta$ -actin promoter/enhancer elements, all CD45<sup>+</sup> cells fluoresced green and not red at all sites examined in unmanipulated Kaede tg mice (Fig. 1A).

To study leukocyte immigration to the gut, we monitored movement of selected phenotypes from a distal lymphoid organ. Preliminary studies revealed very similar immigration of cells from the inguinal LNs (ILNs; lateral iliac LNs per ref. 11) and cervical LNs (CLNs, or mandibular LNs according to the nomenclature of ref. 11) to the gut and gut-draining LNs (Fig. S1). We chose to photoconvert cells in the CLNs in subsequent experiments because of several practical considerations: (i) the increased reproducibility of photoconversion at that site given that CLNs, but not ILNs, can be visualized by eye once the fur has been removed; (ii) even lower nonspecific photoconversion of cells in the peritoneum and gut tissues by targeting the more distant CLNs; and (iii) the larger cell population in the CLNs (see below). Similar to what has been reported for other LNs (12, 14), exposure of the CLNs, through depilated overlying skin, to violet light for 3.5-min photoconverted Kaede in 30–50% of CD45<sup>+</sup> cells at that site, although it remained unconverted at all distal locations examined (Fig. 1B and see below).

To examine immune-cell emigration from the gut, we developed an endoscopic procedure to stereotypically label cells in the descending colon, which is the enteric region richest in

microbial colonization (16) and the site of ulcerative colitis (17). This gut segment is known to host functionally relevant populations of both T helper (Th)17 (18) and regulatory T (Treg) (19) cells. In set-up experiments, transcutaneous exposure of the enteric region to violet light led to weak and diffuse photoconversion, and the endoscope was not able to access the small intestine (SI) and other regions of the colon. Endoscopic exposure of violet light to the descending colon for a total of 5 min resulted in photoconversion of Kaede in 25–35% of CD45<sup>+</sup> cells in the distal large-intestinal lamina propria (LI-LP), but not detectably at other sites, including other regions of the LI-LP, the SI-LP, the Peyer's Patches (PP), and nearby LNs (Fig. 1C and see below).

Subsequent to violet light exposure, most of the Kaede-red<sup>+</sup> CD45<sup>+</sup> cells progressively exited the CLNs or LI-LP and were replaced by incoming Kaede-green<sup>+</sup> cells (Fig. 1D and E and Table S1; see also Table S2), a process previously demonstrated to reflect steady-state leukocyte circulation (12, 14) (and see below). Efflux of Kaede-red<sup>+</sup> immune cells was distinctly more rapid from the LI-LP than from the CLNs, the former near-complete after only 1 d. In general, the major lymphoid subsets circulated more extensively and rapidly than did the myeloid subsets, although this appeared not to be the case for all T-cell classes. For example, Kaede-red<sup>+</sup> conventional T (Tconv) cells exited the CLNs much more effectively than did Kaede-red<sup>+</sup> Treg cells, and photo-tagged Th1 and Th17 cells were both restrained in their exodus (Fig. 1D and E). The various observations are unlikely to reflect substantial violet light-induced cell death in either tissue given near-identical scatter profiles before and after photoconversion.

**Tracking Immigration of Leukocytes to the Gut from a Distant LN.** We began with a time-course experiment designed to evaluate the frequency and rapidity of cell trafficking from the CLNs to various regions of the gut, in comparison with their circulation through extragut lymphoid tissue. CLNs of 13-wk-old Kaede tg mice were exposed to violet light, and tissues were excised for

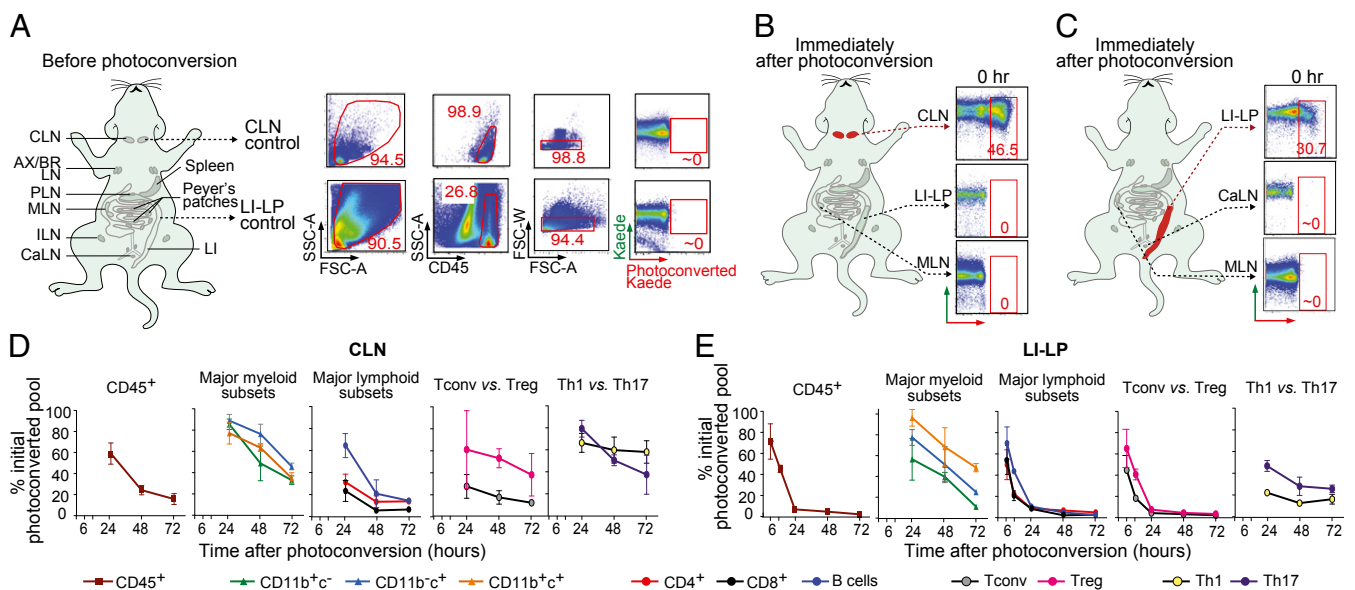


**Fig. 1.** Establishing methodology to track immune cell trafficking into and out of the gut. (A) Lymphoid tissues of an unmanipulated Kaede tg mouse with sample flow cytometry data. (B) CLN cells were labeled (in red), and diverse tissues were immediately harvested and analyzed by flow cytometry for the fraction of Kaede-red<sup>+</sup>CD45<sup>+</sup> cells. Representative dot plots. (C) Same as corresponding B panels except that cells in the descending colon were photo-tagged (in red). (D) Summary plots of rates of egress of cells labeled in the CLNs. Major myeloid subsets were CD11b/c splits; B cells were defined as CD19<sup>+</sup>CD4<sup>-</sup>CD8<sup>-</sup>; Tconv and Treg cells were CD4<sup>+</sup>Foxp3<sup>-</sup> and CD4<sup>+</sup>Foxp3<sup>+</sup> cells, respectively; Th1 or Th17 cells were CD4<sup>+</sup> cells expressing IFN- $\gamma$  or IL-17, respectively. (E) As per D, except egress rates of cells photo-tagged in the descending colon are plotted. For all panels:  $n = 6$ –8 mice from two to three experiments. AX, axial; BR, brachial; PLN, pancreatic lymph nodes.

flow-cytometric analysis of cells containing photoconverted Kaede, immediately or 1–3 d later. That the resulting data reflect cell proliferation to any substantial degree is unlikely given the invariable mean fluorescence intensity of Kaede-red staining in cells examined from 1 to 7 d after exposure to violet light (Fig. S2). Kaede-red<sup>+</sup> CD45<sup>+</sup> cells were detected at all of the locations examined, although relatively few, fractionally, were found in the SI-LP and PPs (Fig. 2A). The kinetics of Kaede-red<sup>+</sup> leukocyte appearance in the LI-LP was very similar to that in the MLNs (jejunal and colic LNs according to ref. 11) or in the ILNs (Fig. 2B).

In general, and as expected, appearance of cells of the major myeloid and lymphoid subsets in the ILNs reflected exodus rates from the CLNs (Fig. 1D vs. Fig. 2C and D). To assess selective migration of the various subsets to the gut, we quantified, over time, the content of photo-tagged cells in the different compartments of gut-associated tissues compared with in the same compartment of the ILNs, the latter being a measure of systemic circulation pools (Fig. 2E and F and Table S3). All of the major myeloid subsets immigrated to the colon to at least some degree, although accumulation of CD11b<sup>+</sup>c<sup>-</sup> and CD11b<sup>-</sup>c<sup>+</sup> cells was relatively disfavored and of CD11b<sup>+</sup>c<sup>+</sup> favored (Fig. 2E). These

differences did not simply parallel variations in relative numbers of cells photoconverted in the CLNs (Tables S1 and S2), exodus rates (Fig. 1D), or differential compartment sizes in the LI-LP vs. CLNs (Table S4). Each of the major lymphoid subsets also trafficked to the LI-LP, with only subtle variations in effectiveness (Fig. 2F).

Examination of CD4<sup>+</sup> T-cell subsets revealed certain more striking differential migratory behaviors. Reflecting their restrained egress from the CLNs (Fig. 1D), the fractional accumulation of Kaede-red<sup>+</sup> Treg cells was lower than that of their Tconv cell counterparts in all tissues examined, levels of Tregs in the LI-LP being particularly low (Fig. 2G). (Note: The Th1 and Th17 compartments in the LI-LP were too small for accurate assessment of immigration from the CLNs.)

**Monitoring Leukocyte Emigration from the Colon.** Next, we tracked the movement of immune cells from the LI to nearby and distant lymphoid organs. The descending colon of 13-wk-old Kaede tg mice was endoscopically exposed to violet light, and various tissues were removed and cytofluorimetrically examined for cells containing photoconverted Kaede, at various time points up to 72 h. By 48 h, cells photo-tagged in the colon were detected at all

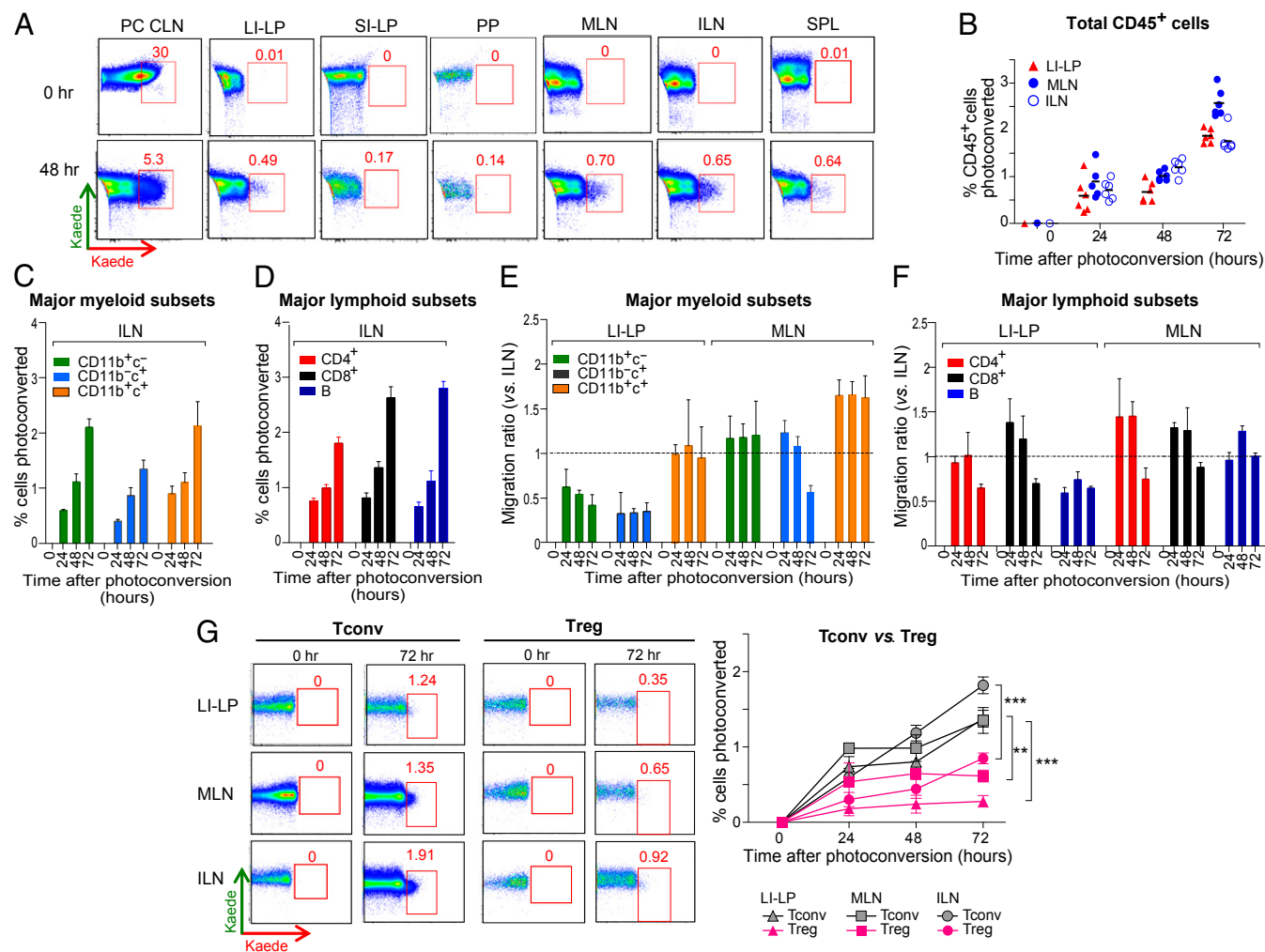


**Fig. 2.** Tracking immigration of immune cells to the gut. (A) Exemplar flow cytometry data from 0 and 48 h after photoconversion of CLNs. Photoconverted CLNs (PC CLNs), several enteric lymphoid tissues (LI-LP, SI-LP, PP, MLN), and control lymphoid tissues (ILN, SPL) are shown. (B–F) Migration of cells to the LI-LP, nearby MLNs and control distal ILNs: total CD45<sup>+</sup> cells (B), CD11b/c splits of myeloid-lineage cells (C, ILN), and major lymphoid-cell subsets (D, ILN). (E and F) Migration of same subsets to LI-LP and MLN, versus the ILN. (G) Similar analyses extended to Tconv vs. Treg cells. Representative dot-plots (Left), summary data (Right). For all panels:  $n = 6–8$  mice from two to three experiments.  $**P < 0.01$ ,  $***P < 0.0011$ .

locations examined, including the SI-LP and other (ascending and transverse) regions of the colon (Fig. 3A, Lower). A comparison with the corresponding dot-plots for the 0-h time points indicates that spurious photoactivation within the nearby regions cannot account for the appearance of cells with photoconverted reporter (Fig. 3A, Upper). Kaede-red<sup>+</sup> CD45<sup>+</sup> cells from the descending colon emerged first and foremost in the caudal LN (CaLN; caudal mesenteric LN per ref. 11), well before their appearance in the MLNs (Fig. 3B), consistent with the aforementioned dye-tracking experiments (10). The rapid accumulation of photo-tagged cells in the CaLN was specific as such cells were not detectable in the adjacent medial iliac LNs. The lower fractional representation of labeled cells in the MLNs and ILNs after flashing the LI-LP versus the CLNs (Fig. 2B) parallels the fewer CD45<sup>+</sup> cells photo-tagged in the former vs. latter tissue (Table S1 vs. Table S2).

Particular immune-cell subsets exhibited distinct patterns of emigration from the colon to neighboring and outlying lymphoid tissues (Fig. 3C–E and Table S5). Unfortunately, the small size of the CaLN precluded studies on subset-specific migration to this node, but it was possible to track the major myeloid and lymphoid subsets to all of the other sites examined. For the myeloid lineage, Kaede-red<sup>+</sup> CD11b<sup>+</sup>c<sup>+</sup> cells consistently accumulated to the highest fractional levels, which, interestingly, did

not reflect either a particularly large starting population of labeled LI-LP cells (Table S2) or particularly effective colonic egress (Fig. 1E). In contrast, photo-tagged CD11b<sup>+</sup>c<sup>+</sup> cells always showed the lowest fractional representation in the lymphoid tissues (Fig. 3C), again not reflective of either the size of the starting labeled LI-LP population or the egress rates (Fig. 1E and Table S2). The fraction of photo-tagged lymphoid cells in nearby and distal lymphoid organs was, in general, distinctly lower than that of myeloid cells (compare Fig. 3C and D). This result was unexpected given that more lymphocytes were labeled within (Table S2) and that lymphocytes egressed faster from (Fig. 1D) the LI. However, the differences might be explained—at least partially—by the fact that, in general, the relative sizes of lymphoid cell compartments in lymphoid organs versus in the LI-LP are greater than is the case for the corresponding myeloid cell compartments (Table S4). In contrast to what had been seen for migration to the LI-LP from the CLNs, circulation of Tregs from the distal LI to other locations, although quite low, was slightly more effective than trafficking of Tconv cells (Fig. 3E). This difference is also likely to reflect relative compartment sizes: the relative size of the Tconv cell compartments in lymphoid organs versus in the LI-LP is greater than is the case for the corresponding Treg compartments (Table S4). Again, the Th1 and

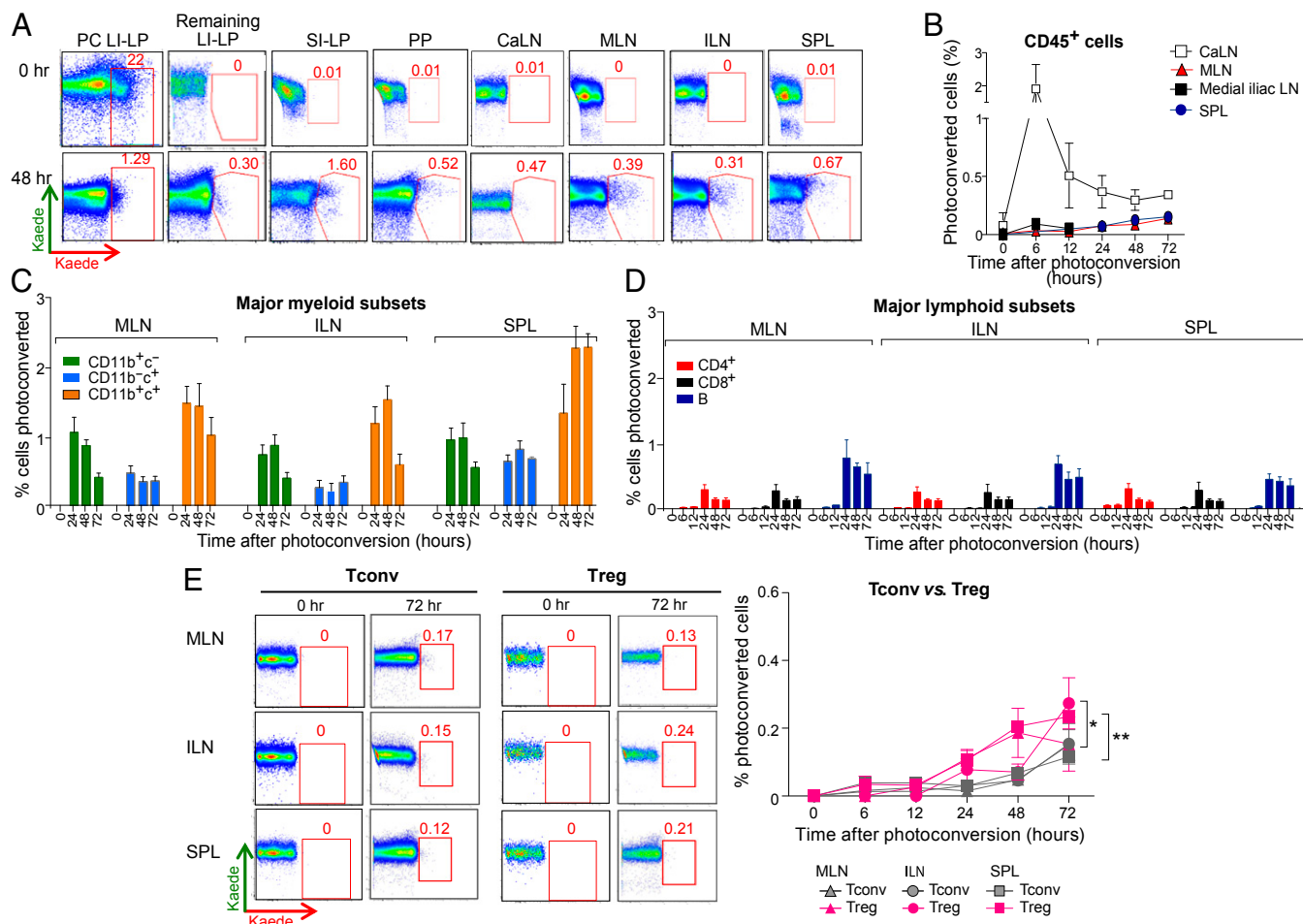


**Fig. 3.** Monitoring immune cell emigration from the colon. (A) As for Fig. 2A, except after photoconversion of descending colon. Additional sites examined were unconverted (i.e., ascending and transverse) regions of the colon (Remaining LI-LP) and the CaLN. PC LI-LP refers to the photoconverted descending colon. (B–E) Migration of cells to the gut-associated CaLN and MLN, control medial iliac LN and distal ILN, and spleen: total CD45<sup>+</sup> cells (B), CD11b/c splits of myeloid-lineage cells (C), and major lymphoid-cell subsets (D). (E) Similar analyses extended to Tconv vs. Treg cells. Representative dot-plots (Left), summary data (Right). For all panels:  $n = 6$ –8 mice from two to three experiments. \* $P < 0.05$ , \*\* $P < 0.01$ .

Th17 compartments in the LI-LP were too small to permit accurate tracking after dispersal through the body.

#### Linking Colonic T Cells to a Gut-Distal Autoinflammatory Disease.

Finally, we were interested in potentially tying leukocyte trafficking from the gut to pathogenesis. K/BxN TCR tg mice are a model of autoinflammatory arthritis (reviewed in ref. 20). The K/BxN disease depends on excessive production of autoantibodies (autoAbs) to glucose-6-phosphate isomerase (GPI), primarily in the spleen (21). Circulating GPI and anti-GPI autoAbs form immune complexes that deposit on joints, where they induce activation of the innate immune system and ultimately inflammation (22). The requisite high level of circulating anti-GPI autoAbs depends critically on an interaction between B and Th17 lymphocytes in the spleen which, in turn, relies on induction of a robust Th17 compartment by the intestinal microbiota (4). We sought evidence that gut-derived Th17 cells can contribute to the gut-distal autoinflammatory disease of K/BxN mice.

Violet light was shone on the descending colon of 3.5-wk-old K/BxN mice, the age at which Th17 cells start to accumulate in the spleen and anti-GPI autoAb production begins (4). Seventy-two hours later, few CD4<sup>+</sup> T cells with photoconverted Kaede remained in the LI-LP, although slightly more IL-17A producers than nonproducers (Fig. 4*A* and *B*). Although we could pick up both types of CD4<sup>+</sup> cell in the spleen at that time point, there was a higher fractional representation of Th17 cells (Fig. 4*C*). Moreover, the fraction of Kaede-red<sup>+</sup> Th17 cells in the spleen of individual mice correlated well with the titer of serum anti-GPI autoAbs (Fig. 4*D*). Thus, we have evidenced gut-derived Th17 cells in the spleen of K/BxN mice. Note that, in contrast, there was minimal exodus of Th17 cells from the gut in the above-described experiments on nonarthritic mice.

#### Discussion

The Kaede tg mouse offers a novel, minimally perturbant and sensitive means to track the migration of essentially any leukocyte cell-type definable by surface-displayed or intracellular markers, into or out of the gut from a defined point of origin. Although experiments on emigration from the gut were limited

to the descending colon in this report, we have recently been able to adapt the system for other intestinal regions via gentle externalization, light-flashing, and reinsertion of small loops of tissue. Thus, the Kaede approach may prove more widely applicable and less artifact-prone than many existing technologies for tracking gut-related cell migration. Many of the prevailing systems require cell transfer, and so one is limited to following movement of the specific cell-types that were transferred or a particular fraction of them. In addition, there may be artifacts resulting from removal of cells from their supporting niche, or from purification processes or mAb binding, and possibly additional issues related to excessive cell numbers.

We therefore undertook a comprehensive analysis of leukocyte immigration to the gut and emigration from the descending colon. The goal was to provide a wide-angle view of gut-associated trafficking in a given individual, and to visualize how this might evolve with a pathologic shift of the homeostatic balance. Our major findings were: (i) all major myeloid and lymphoid subsets migrated to the colon to a readily detectable degree, in fact not very differently from their propensity to traffic through the lymphoid organs; (ii) unexpectedly, all of the major immune-cell subsets also trafficked out of the descending colon to both nearby and distal locations, exit from the colon being distinctly more rapid than from the CLNs; (iii) the CaLN was the primary site of immune-cell drainage from the descending colon; (iv) Tconv and Treg cells showed different migratory patterns (e.g., the former circulated more effectively out of the CLNs); (v) because of their low numbers, it was difficult to reliably detect Th17 cell migration at steady state; however, in the inflammatory arthritis setting it was possible to document colon-derived Th17 cells in the spleen, the dominant site of autoAb production. A few of these points bear further discussion.

First, our results have rehighlighted the importance of the CaLN. Many investigators are rather loose in their identification and naming of the LNs in experimental mice, especially those associated with the gastrointestinal tract. Recognizing this problem, Van den Broeck et al. proposed adopting a more precise designation of murine LNs (11), one which was recently validated in an independent study (23). According to this nomenclature, the gastrointestinal tract is serviced by a set of nodes, termed (proximally to distally): the gastric, pancreaticoduodenal, jejunal, colic, and caudal mesenteric LNs. Investigators commonly consider that the gastrointestinal tract is drained by the “mesenteric lymph nodes,” generally referring to the jejunal plus colic LNs. However, long ago, dye-tracking studies established that things are really much more complex (10). Specific regions of the gut are directly drained by particular LNs: for example, distal segments of the jejunal-colic LN tract drain the distal ileum, cecum, and ascending colon; the pancreaticoduodenal LNs service the duodenum and transverse colon; and the CaLN drains the descending colon. Our data derived from the Kaede system are consistent with these long-standing but often ignored findings: immune cells photo-tagged in the descending colon went first and foremost to the CaLN. It may prove useful to embrace such distinctions in future studies aimed at monitoring translocation of microbes from the gastrointestinal tract (cf. ref. 9) or at defining enteric homing receptors (cf. ref. 24), for example.

Second, our data underscore the tight relationship between the Th17 compartment and the gut. In both mice and humans, the vast majority of this Th subset resides in the gastrointestinal tract, in particular the SI-LP, but extending as far as the distal LI-LP (reviewed in ref. 25). The fractional representation of Th17 cells in LNs and the spleen is low, even in the gut-draining MLNs. Nonetheless, IL-17-producing cells are known to be critical participants in a number of gut-distal immune responses, whether autoimmune, inflammatory, or antimicrobial. Currently, it is unclear to what extent there is communication between the

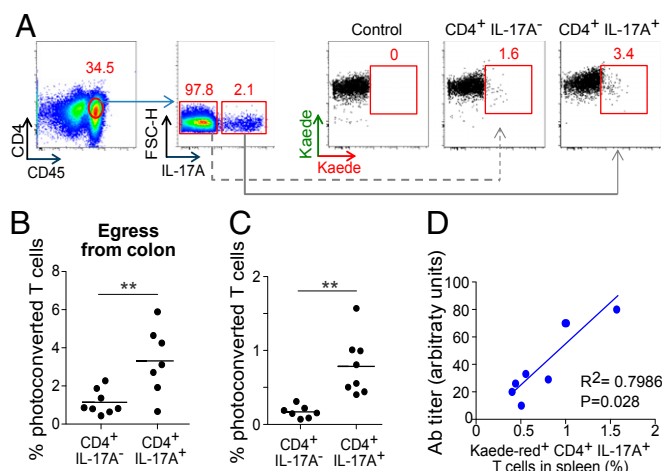


**Fig. 4.** Linking colonic T cells to a gut-distal autoinflammatory disease. (*A* and *B*) Seventy-two hours after exposure of the descending colon of 24-d-old K/BxN mice to violet light, IL-17A-producing and -nonproducing CD4<sup>+</sup> T cells in the PC LI-LP were enumerated, as a confirmation of egress. (*A*) Representative dot plots; (*B*) summary data. (*C*) Immigration to the spleen in these same mice.  $n = 7-8$  from three independent experiments. (*D*) The proportion of splenic IL-17<sup>+</sup>CD4<sup>+</sup> cells that were Kaede-red<sup>+</sup> plotted against the anti-GPI autoAb titer, an early (required) disease indicator in K/BxN mice.  $**P < 0.01$ .

Th17 populations residing in the gut and circulating outside. Although at steady state there were too few Th17 cells in either the CLNs or gut to permit accurate tracking to individual tissues, efflux measurements evidenced their entry into the circulation, from both the CLNs and the LI-LP (Fig. 1 *D* and *E*). Analysis of the K/BxN arthritis model revealed gut-derived Th17 cells in the spleen, where they drove the production of pathogenic auto Abs.

Although this study sought a broad perspective on leukocyte homing into and out of the gut, the Kaede tg mouse system has great potential for addressing a range of more specific issues, focusing, for example, on precisely which monocyte/macrophage or dendritic cell subsets transit to the MLNs or CaLN under defined conditions; or what the dynamic pathway of cell movement out of different segments of the intestine is; or how the transcriptome of cells arriving at a particular site evolve over time. The area of gut-associated leukocyte trafficking has obvious clinical importance in the contexts of inflammatory bowel disease, vaccine design, and probiotics.

## Methods

**Mice.** The Kaede tg mouse line (Kaede.NOD) was obtained from O. Kanagawa (RIKEN, Wako, Japan). K/BxN animals carrying the Kaede reporter were generated by crossing KRN T-cell receptor tg mice on the C57BL/6 background (KRNB6) (26) with Kaede.NOD mice. All animals were bred and maintained in our specific pathogen-free facility at Harvard Medical School. Experiments were conducted under protocols approved by Harvard Medical School's Institutional Animal Care and Use Committee. Typically, six to eight male mice were used per condition, spread over more than two independent experiments. In our colony, male mice of the NOD strain rarely develop diabetes and only at an advanced age.

**Photoconversion Procedures.** Mice were anesthetized with ketamine:xylazine in combination (10 mg/kg:2 mg/kg i.p.) or 3% (vol/vol) isoflurane, delivered in 2 L/min of 100% O<sub>2</sub>. For photoconversion of Kaede in CLN cells, overlying fur was removed using depilatory cream. Mice were placed on their backs with an aluminum foil blanket covering all but the depilated area, and violet light (Electra Pro Series Violet Handheld Laser; Laserglow Technologies) was shone (405 nm; peak power <5 mW; sustained power: 0.5–4.9 mW) onto the exposed area for a period of 3.5 min (direct exposure) or 5 min (via fiberoptics). To manipulate the size of the light field so that both CLNs could be exposed, we attached a lens to the laser to defocus the beam, and the source of the defocused light beam was positioned 28 cm above the mouse; beam

diameter was 1.5 cm. For cell photoconversion in the descending colon, a custom-built fiberoptic endoscope (ZIBRA Corporation) was coupled to the handheld 405-nm laser, via an in-house, custom-made connection device (fixed mounts were purchased from Thorlabs). After cleansing the colon of fecal pellets with PBS, we inserted the fiberoptic endoscope through the anus into the descending colon to a depth of 2.5 cm. The laser was switched on, thereby exposing the inner colon to violet light (beam diameter was 3.5 mm). Subsequently, the endoscope was gently retracted, pausing at 2-mm increments for 30-s light pulses at each interval (for a total of 5 min).

**LI-LP, SI-LP, and PP Cell Isolation.** LI and SI were harvested and fat and PPs removed. LI and SI were incubated in extraction medium (0.01% DTT, 1 mM EDTA, 2% FCS, RPMI-1640 medium for 15 min with continual stirring, at 37 °C). Tissues were then washed and residual mucus removed. Next, all tissues, including PPs, were cut into 1-mm<sup>2</sup> pieces and incubated in digestion medium (2% FBS, 0.05% Dispase, 0.15% Type II Collagenase, RPMI-1640) for 15–30 min at at 37 °C. Following digestion, the preparation was filtered and washed twice.

**Flow Cytometry.** For surface phenotype analyses by flow cytometry (LSRII), fluorophore-labeled mAbs specific for CD45, CD4 (BD Biosciences), CD8, CD19, CD11b, or CD11c were obtained from BioLegend (unless otherwise noted). Intracellular Foxp3 was detected with a staining-buffer set (eBioscience), according to the manufacturer's instructions. For intracellular cytokine analysis, cells were stimulated with 50 ng/mL phorbol 12 myristate 13-acetate and 1 μM ionomycin (both from Sigma) in the presence of BD GolgiPlug (1:1,000 dilution) for 4 h at 37 °C, 5% CO<sub>2</sub>. Intracellular cytokines were then stained using a BD Cytofix/Cytoperm kit, as per the manufacturer's directions.

**ELISAs.** Anti-GPI titers in blood collected from 4-wk-old K/BxN.Kaede mice were quantified as previously reported (27). For correlation analysis, serum dilution at a change in absorbance of 1 was plotted against proportion of photoconverted Th17 cells in spleen.

**Statistical Analyses.** Statistical significance, indicated by asterisks, was determined by Student *t* test (two-tailed, unpaired). *P* values < 0.05 were considered significant: \**P* < 0.05, \*\**P* < 0.01, \*\*\**P* < 0.001.

**ACKNOWLEDGMENTS.** We thank Dr. O. Kanagawa for providing the Kaede line. This work was supported by a National Institutes of Health Grant P01 AI054904 (to D.M., C.B., and R.W.); and Juvenile Diabetes Research Foundation Fellowship 3-2011-413 (to A.M.M.). R.U. is a Howard Hughes Medical Institute Medical Research Fellow.

- Ivanov II, Honda K (2012) Intestinal commensal microbes as immune modulators. *Cell Host Microbe* 12(4):496–508.
- Hart AL, et al. (2010) Homing of immune cells: Role in homeostasis and intestinal inflammation. *Inflamm Bowel Dis* 16(11):1969–1977.
- Kriegl MA, et al. (2011) Naturally transmitted segmented filamentous bacteria segregate with diabetes protection in nonobese diabetic mice. *Proc Natl Acad Sci USA* 108(28):11548–11553.
- Wu HJ, et al. (2010) Gut-residing segmented filamentous bacteria drive autoimmune arthritis via T helper 17 cells. *Immunity* 32(6):815–827.
- Bain CC, et al. (2013) Resident and pro-inflammatory macrophages in the colon represent alternative context-dependent fates of the same Ly6Chi monocyte precursors. *Mucosal Immunol* 6(3):498–510.
- Rivollier A, He J, Kole A, Valatas V, Kelsall BL (2012) Inflammation switches the differentiation program of Ly6Chi monocytes from anti-inflammatory macrophages to inflammatory dendritic cells in the colon. *J Exp Med* 209(1):139–155.
- Zigmond E, et al. (2012) Ly6C hi monocytes in the inflamed colon give rise to proinflammatory effector cells and migratory antigen-presenting cells. *Immunity* 37(6):1076–1090.
- Mowat AM (2003) Anatomical basis of tolerance and immunity to intestinal antigens. *Nat Rev Immunol* 3(4):331–341.
- Diehl GE, et al. (2013) Microbiota restricts trafficking of bacteria to mesenteric lymph nodes by CX(3)CR1(hi) cells. *Nature* 494(7435):116–120.
- Carter PB, Collins FM (1974) The route of enteric infection in normal mice. *J Exp Med* 139(5):1189–1203.
- Van den Broeck W, Derore A, Simoens P (2006) Anatomy and nomenclature of murine lymph nodes: Descriptive study and nomenclature standardization in BALB/cAnNCrl mice. *J Immunol Methods* 312(1–2):12–19.
- Tomura M, et al. (2008) Monitoring cellular movement in vivo with photoconvertible fluorescence protein “Kaede” transgenic mice. *Proc Natl Acad Sci USA* 105(31):10871–10876.
- Tomura M, et al. (2010) Activated regulatory T cells are the major T cell type emigrating from the skin during a cutaneous immune response in mice. *J Clin Invest* 120(3):883–893.
- Tomura M, Itoh K, Kanagawa O (2010) Naive CD4+ T lymphocytes circulate through lymphoid organs to interact with endogenous antigens and upregulate their function. *J Immunol* 184(9):4646–4653.
- Bromley SK, Yan S, Tomura M, Kanagawa O, Luster AD (2013) Recirculating memory T cells are a unique subset of CD4+ T cells with a distinct phenotype and migratory pattern. *J Immunol* 190(3):970–976.
- Dethlefsen L, McFall-Ngai M, Relman DA (2007) An ecological and evolutionary perspective on human-microbe mutualism and disease. *Nature* 449(7164):811–818.
- Strober W, Fuss IJ (2011) Proinflammatory cytokines in the pathogenesis of inflammatory bowel diseases. *Gastroenterology* 140(6):1756–1767.
- Atarashi K, et al. (2008) ATP drives lamina propria T(H)17 cell differentiation. *Nature* 455(7214):808–812.
- Atarashi K, et al. (2011) Induction of colonic regulatory T cells by indigenous Clostridium species. *Science* 331(6015):337–341.
- Monach PA, Mathis D, Benoist C (2008) The K/BxN arthritis model. *Curr Protoc Immunol* Chapter 15:Unit 15.22.
- Maccioni M, et al. (2002) Arthritogenic monoclonal antibodies from K/BxN mice. *J Exp Med* 195(8):1071–1077.
- Matsumoto I, et al. (2002) How antibodies to a ubiquitous cytoplasmic enzyme may provoke joint-specific autoimmune disease. *Nat Immunol* 3(4):360–365.
- Shao L, et al. (2013) Lymphatic mapping of mice with systemic lymphoproliferative disorder: Usefulness as an inter-lymph node metastasis model of cancer. *J Immunol Methods* 389(1–2):69–78.
- Kim SV, et al. (2013) GPR15-mediated homing controls immune homeostasis in the large intestine mucosa. *Science* 340(6139):1456–1459.
- Littman DR, Rudensky AY (2010) Th17 and regulatory T cells in mediating and restraining inflammation. *Cell* 140(6):845–858.
- Koukoff V, et al. (1996) Organ-specific disease provoked by systemic autoimmunity. *Cell* 87(5):811–822.
- Matsumoto I, Staub A, Benoist C, Mathis D (1999) Arthritis provoked by linked T and B cell recognition of a glycolytic enzyme. *Science* 286(5445):1732–1735.

# Supporting Information

Morton et al. 10.1073/pnas.1405634111

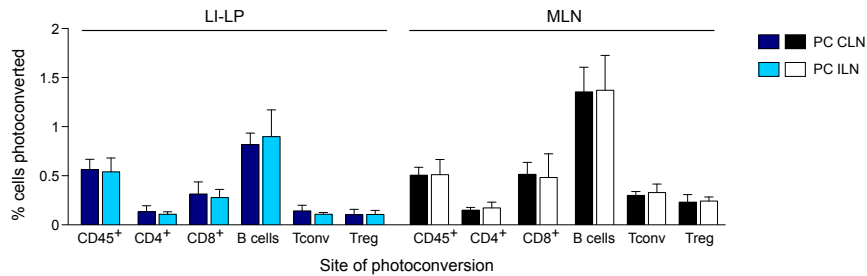


**Fig. S1.** Immune cells migrate similarly to gut and gut-draining lymph nodes (LNs) from inguinal LNs (ILNs) and cervical LNs (CLNs). The presence of Kaede-red<sup>+</sup> cells in the large-intestinal lamina propria (LI-LP) and mesenteric LNs (MLNs) was detected by flow cytometry 72 h after photoconversion of the ILNs or CLNs. No significant differences observed. three mice per group. PC CLNs, photoconverted CLNs; Tconv, conventional T cells; Treg, regulatory T cells.

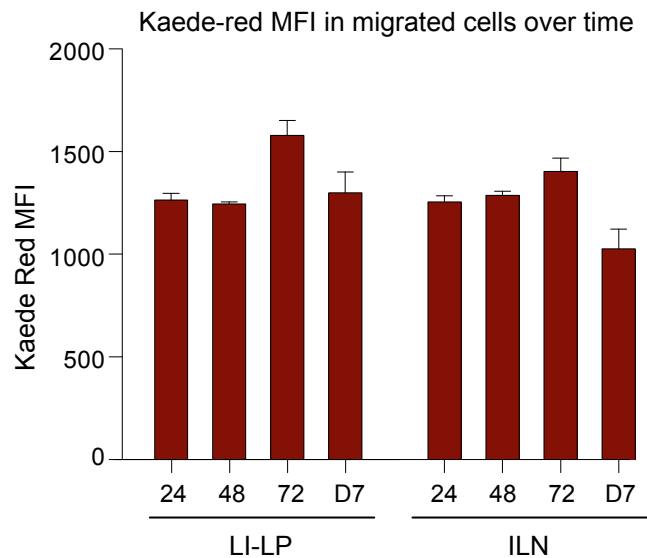


**Fig. S2.** Immigration values not greatly influenced by proliferation. The mean fluorescence intensity (MFI) of Kaede-red in CD45<sup>+</sup> cells of the LI-LP or ILN was measured at multiple time points (24, 48, 72 h, and day 7) after exposure of the CLNs to violet light. No significant differences observed.

**Table S1. Exit of photoconverted cells from the sites of photoconversion: CLN**

CLN	Time after photoconversion (h)			
	0	24	48	72
CD45 <sup>+</sup>	<b>2,967,303</b>	<b>1,752,111</b>	<b>719,993</b>	<b>468,378</b>
	359,560	149,798	64,560	77,000
CD11b <sup>+</sup> c <sup>-</sup>	<b>109,407</b>	<b>93,520</b>	<b>53,338</b>	<b>36,074</b>
	8,129	2,696	8,900	2,201
CD11b <sup>-</sup> c <sup>+</sup>	<b>35,797</b>	<b>31,808</b>	<b>27,351</b>	<b>16,403</b>
	2,417	1,069	1,643	557
CD11b <sup>+</sup> c <sup>+</sup>	<b>15,013</b>	<b>11,584</b>	<b>9,521</b>	<b>5,238</b>
	827	765	262	380
CD4 <sup>+</sup>	<b>951,299</b>	<b>297,806</b>	<b>128,073</b>	<b>132,289</b>
	98,618	34,835	25,606	2,230
CD8 <sup>+</sup>	<b>364,740</b>	<b>82,714</b>	<b>20,304</b>	<b>23,423</b>
	29,272	17,614	3,245	2,308
B cells	<b>1,366,719</b>	<b>920,957</b>	<b>285,155</b>	<b>197,999</b>
	78,896	77,680	85,772	8,581
Tconv	<b>702,355</b>	<b>194,750</b>	<b>124,096</b>	<b>89,736</b>
	57,946	37,678	21,487	3,475
Treg	<b>113,366</b>	<b>70,068</b>	<b>60,370</b>	<b>52,034</b>
	8,348	23,782	4,907	2,918
Th1	<b>22,554</b>	<b>14,967</b>	<b>13,492</b>	<b>13,098</b>
	2,755	967	1,335	1,149
Th17	<b>2,593</b>	<b>2,055</b>	<b>1,310</b>	<b>971</b>
	281	99	64	231

Number of photoconverted cells in the sites of photoconversion at the time points indicated. Boldface entries indicate the mean; nonboldface indicates  $\pm$ SD.

**Table S2. Exit of photoconverted cells from the sites of photoconversion: LI-LP**

LI-LP	Time after photoconversion (h)					
	0	6	12	24	48	72
CD45 <sup>+</sup>	<b>561,157</b>	<b>419,939</b>	<b>268,810</b>	<b>45,710</b>	<b>32,424</b>	<b>18,609</b>
	166,038	84,453	17,439	13,177	10,301	2,558
CD11b <sup>+</sup> c <sup>-</sup>	<b>14,100</b>	ND	ND	<b>7,976</b>	<b>5,597</b>	<b>1,543</b>
	3,900			2,824	597	264
CD11b <sup>-</sup> c <sup>+</sup>	<b>11,150</b>	ND	ND	<b>8,640</b>	<b>5,728</b>	<b>2,798</b>
	3,233			843	1,925	307
CD11b <sup>+</sup> c <sup>+</sup>	<b>6,522</b>	ND	ND	<b>6,287</b>	<b>4,457</b>	<b>3,165</b>
	1,891			522	1,208	259
CD4 <sup>+</sup>	<b>92,152</b>	<b>46,059</b>	<b>20,764</b>	<b>7,884</b>	<b>6,296</b>	<b>4,536</b>
	15,600	11,221	740	1,573	1,305	870
CD8 <sup>+</sup>	<b>23,860</b>	<b>13,022</b>	<b>4,935</b>	<b>1,977</b>	<b>533</b>	<b>663</b>
	4,104	2,820	955	314	110	100
B cells	<b>289,485</b>	<b>203,833</b>	<b>126,538</b>	<b>30,396</b>	<b>14,046</b>	<b>6,824</b>
	49,916	38,118	5,246	4,111	5,359	1,476
Tconv	<b>73,075</b>	<b>32,798</b>	<b>13,411</b>	<b>4,316</b>	<b>2,485</b>	<b>1,731</b>
	12,569	8,770	317	395	589	114
Treg	<b>13,260</b>	<b>8,661</b>	<b>5,415</b>	<b>1,024</b>	<b>816</b>	<b>476</b>
	2,281	2,074	579	242	45	99
Th1	<b>3,797</b>	ND	ND	<b>840</b>	<b>475</b>	<b>613</b>
	653			44	83	171
Th17	<b>530</b>	ND	ND	<b>248</b>	<b>149</b>	<b>136</b>
	91			27	44	18

Number of photoconverted cells in the sites of photoconversion at the time points indicated. Boldface entries indicate the mean; nonboldface indicates  $\pm$ SD.

**Table S3. Leukocyte trafficking from the CLNs to gut-associated and control tissues**

CLN	Time after photoconversion (h)			
	0	24	48	72
<b>LI-LP</b>				
CD45 <sup>+</sup>	0	<b>22,029</b> ± 13,841	<b>24,980</b> ± 8,152	<b>69,613</b> ± 5,620
CD11b <sup>+</sup> c <sup>-</sup>	0	<b>394</b> ± 240	<b>616</b> ± 55	<b>909</b> ± 580
CD11b <sup>-</sup> c <sup>+</sup>	0	<b>109</b> ± 146	<b>212</b> ± 60	<b>315</b> ± 190
CD11b <sup>+</sup> c <sup>+</sup>	0	<b>321</b> ± 49	<b>392</b> ± 275	<b>560</b> ± 244
CD4 <sup>+</sup>	0	<b>7,080</b> ± 2,732	<b>10,168</b> ± 4,198	<b>12,167</b> ± 3,355
CD8 <sup>+</sup>	0	<b>2,328</b> ± 442	<b>3,241</b> ± 502	<b>3,950</b> ± 1,295
B cells	0	<b>7,334</b> ± 1,197	<b>15,723</b> ± 9,339	<b>32,265</b> ± 4,182
Tconv	0	<b>6,329</b> ± 2,854	<b>6,880</b> ± 2567	<b>11,808</b> ± 2,319
Treg	0	<b>406</b> ± 210	<b>541</b> ± 216	<b>314</b> ± 214
<b>MLN</b>				
CD45 <sup>+</sup>	0	<b>63,957</b> ± 44,122	<b>144,318</b> ± 14,989	<b>366,789</b> ± 42,863
CD11b <sup>+</sup> c <sup>-</sup>	0	<b>1,280</b> ± 465	<b>2,358</b> ± 193	<b>4,463</b> ± 1,532
CD11b <sup>-</sup> c <sup>+</sup>	0	<b>1,405</b> ± 284	<b>2,591</b> ± 308	<b>2,634</b> ± 1,248
CD11b <sup>+</sup> c <sup>+</sup>	0	<b>973</b> ± 218	<b>1,270</b> ± 143	<b>2,514</b> ± 490
CD4 <sup>+</sup>	0	<b>36,498</b> ± 5,966	<b>57,902</b> ± 11,224	<b>68,049</b> ± 14,087
CD8 <sup>+</sup>	0	<b>13,542</b> ± 848	<b>27,053</b> ± 10,576	<b>35,734</b> ± 7,453
B cells	0	<b>10,985</b> ± 2,041	<b>17,413</b> ± 6,995	<b>43,533</b> ± 4,666
Tconv	0	<b>47,525</b> ± 5,168	<b>47,557</b> ± 14,770	<b>65,353</b> ± 18,503
Treg	0	<b>1,752</b> ± 818	<b>2,101</b> ± 152	<b>1,992</b> ± 252
<b>ILN</b>				
CD45 <sup>+</sup>	0	<b>33,506</b> ± 9,552	<b>56,537</b> ± 7,923	<b>82,920</b> ± 11,667
CD11b <sup>+</sup> c <sup>-</sup>	0	<b>279</b> ± 17	<b>526</b> ± 113	<b>991</b> ± 172
CD11b <sup>-</sup> c <sup>+</sup>	0	<b>190</b> ± 28	<b>408</b> ± 119	<b>637</b> ± 178
CD11b <sup>+</sup> c <sup>+</sup>	0	<b>84</b> ± 23	<b>104</b> ± 28	<b>201</b> ± 100
CD4 <sup>+</sup>	0	<b>8,764</b> ± 6,092	<b>16,219</b> ± 3,633	<b>33,687</b> ± 5,183
CD8 <sup>+</sup>	0	<b>2,891</b> ± 1,777	<b>6,894</b> ± 789	<b>13,324</b> ± 2,445
B cells	0	<b>31,883</b> ± 4,895	<b>110,262</b> ± 18,222	<b>153,267</b> ± 11,080
Tconv	0	<b>10,223</b> ± 5,141	<b>20,381</b> ± 4,003	<b>31,295</b> ± 4,691
Treg	0	<b>356</b> ± 274	<b>523</b> ± 331	<b>1,003</b> ± 205

Mean number (boldface) ± SD of photoconverted cells detected in the LI-LP, MLN, and ILN at multiple time points after photoconversion of the CLNs.

**Table S4. Compartment sizes**

	CLNs			LI-LP			MLNs			ILNs			Spleen		
	Mean	SD	% CD45 <sup>+</sup>	Mean	SD	% CD45 <sup>+</sup>	Mean	SD	% CD45 <sup>+</sup>	Mean	SD	% CD45 <sup>+</sup>	Mean	SD	% CD45 <sup>+</sup>
CD45 <sup>+</sup>	712.72	19.91	100.00	371.63	72.96	100.00	1424.42	40.02	100.00	475.14	17.45	100.00	6478.07	324.52	100.00
CD11b <sup>+</sup> c <sup>-</sup>	18.53	0.52	2.60	10.41	2.04	2.80	18.52	0.52	1.30	4.75	0.17	1.00	213.78	10.71	3.30
CD11b <sup>-</sup> c <sup>+</sup>	5.70	0.16	0.80	7.43	1.46	2.00	28.49	0.80	2.00	4.75	0.17	1.00	71.26	3.57	1.10
CD11b <sup>+</sup> c <sup>+</sup>	2.14	0.06	0.30	3.72	0.73	1.00	7.12	0.20	0.50	0.95	0.03	0.20	32.39	1.62	0.50
CD4 <sup>+</sup>	248.01	6.93	34.80	102.96	20.21	27.71	504.77	14.18	35.44	188.41	6.92	39.65	1633.41	81.83	25.21
CD8 <sup>+</sup>	79.56	2.22	11.16	21.69	4.26	5.84	152.84	4.29	10.73	51.12	1.88	10.76	536.55	26.88	8.28
B cells	272.88	7.62	38.29	179.06	35.15	48.18	569.39	16.00	39.97	156.72	5.75	32.98	2952.74	147.92	45.58
Tconv	203.48	5.68	28.55	85.97	16.88	23.13	483.35	13.58	33.93	173.58	6.37	36.53	1448.93	72.59	22.37
Treg	25.66	0.72	3.60	11.29	2.22	3.04	32.52	0.91	2.28	11.93	0.44	2.51	114.45	5.73	1.77
Th1	4.92	0.14	0.69	3.36	0.66	0.90	8.75	0.25	0.61	2.97	0.11	0.63	199.42	9.99	3.08
Th17	0.56	0.02	0.08	0.46	0.09	0.12	1.08	0.03	0.08	0.11	< 0.01	0.02	5.52	0.28	0.09
Sum	626.82			325.27			1281.12			406.71			5440.11		

Sum is major myloid plus major lymphoid. Compartment sizes: # (×10<sup>4</sup>) and SD (×10<sup>4</sup>) and % CD45<sup>+</sup> for total cells in each compartment.

**Table S5. Leukocyte trafficking from the gut to other tissues**

	Time after photoconversion (h)			
	0	24	48	72
<b>MLN</b>				
CD45 <sup>+</sup>	0	<b>67,973</b> ± 35,565	<b>37,719</b> ± 11,548	<b>37,932</b> ± 27,795
CD11b <sup>+</sup> c <sup>-</sup>	0	<b>1,938</b> ± 888	<b>1,585</b> ± 312	<b>748</b> ± 245
CD11b <sup>-</sup> c <sup>+</sup>	0	<b>1,323</b> ± 658	<b>976</b> ± 408	<b>1,016</b> ± 406
CD11b <sup>+</sup> c <sup>+</sup>	0	<b>1,039</b> ± 386	<b>1,011</b> ± 457	<b>716</b> ± 402
CD4 <sup>+</sup>	0	<b>14,488</b> ± 8,296	<b>7,042</b> ± 2,382	<b>6,535</b> ± 3,957
CD8 <sup>+</sup>	0	<b>9,816</b> ± 12,668	<b>1,899</b> ± 844	<b>2,107</b> ± 1,481
B cells	0	<b>43,512</b> ± 31,143	<b>34,525</b> ± 6,429	<b>29,705</b> ± 19,312
Tconv	0	<b>723</b> ± 131	<b>2,346</b> ± 282	<b>8,482</b> ± 1,800
Treg	0	<b>361</b> ± 76	<b>606</b> ± 236	<b>499</b> ± 260
<b>ILN</b>				
CD45 <sup>+</sup>	0	<b>17,524</b> ± 11,725	<b>10,204</b> ± 4,156	<b>10,471</b> ± 5,997
CD11b <sup>+</sup> c <sup>-</sup>	0	<b>346</b> ± 147	<b>410</b> ± 141	<b>187</b> ± 87
CD11b <sup>-</sup> c <sup>+</sup>	0	<b>124</b> ± 111	<b>102</b> ± 101	<b>158</b> ± 100
CD11b <sup>+</sup> c <sup>+</sup>	0	<b>112</b> ± 32	<b>144</b> ± 37	<b>55</b> ± 25
CD4 <sup>+</sup>	0	<b>4,717</b> ± 3,310	<b>2,463</b> ± 747	<b>2,303</b> ± 1,202
CD8 <sup>+</sup>	0	<b>1,242</b> ± 1,391	<b>700</b> ± 374	<b>699</b> ± 467
B cells	0	<b>10,554</b> ± 3,972	<b>6,951</b> ± 3,821	<b>7,421</b> ± 4,503
Tconv	0	<b>539</b> ± 114	<b>798</b> ± 85	<b>2,673</b> ± 1,037
Treg	0	<b>93</b> ± 39	<b>84</b> ± 28	<b>326</b> ± 90
<b>SPL</b>				
CD45 <sup>+</sup>	0	<b>282,055</b> ± 125,540	<b>146,404</b> ± 53,060	<b>142,764</b> ± 115,095
CD11b <sup>+</sup> c <sup>-</sup>	0	<b>20,044</b> ± 8,031	<b>20,651</b> ± 9,087	<b>11,608</b> ± 3,885
CD11b <sup>-</sup> c <sup>+</sup>	0	<b>4,492</b> ± 1,473	<b>5,749</b> ± 1,631	<b>4,762</b> ± 455
CD11b <sup>+</sup> c <sup>+</sup>	0	<b>4,259</b> ± 1,901	<b>7,272</b> ± 2,017	<b>7,307</b> ± 1,381
CD4 <sup>+</sup>	0	<b>49,092</b> ± 29,030	<b>22,129</b> ± 7,677	<b>16,488</b> ± 8,929
CD8 <sup>+</sup>	0	<b>15,019</b> ± 14,281	<b>6,706</b> ± 2,607	<b>6,038</b> ± 3,644
B cells	0	<b>131,277</b> ± 53,256	<b>122,463</b> ± 38,870	<b>102,105</b> ± 68,243
Tconv	0	<b>4,300</b> ± 772	<b>9,894</b> ± 4,378	<b>16,810</b> ± 2,750
Treg	0	<b>1,220</b> ± 711	<b>2,362</b> ± 392	<b>2,689</b> ± 412

Mean number (boldface) ± SD of photoconverted cells detected in MLN, ILN, and spleen at different time points following photoconversion of the descending colon.